CrystEngComm

Accepted Manuscript

This article can be cited before page numbers have been issued, to do this please use: Y. Endo, M. Kondo, T. Nakamura, S. Hattori, A. Sekine, S. Kojo and K. Shinozaki, *CrystEngComm*, 2026, DOI: 10.1039/D6CE00194G.

ROYAL SOCIETY OF CHEMISTRY

rsc.li/crystengcomm

View Article Online
DOI: 10.1039/D6CE00194G

Structure and Luminescence Colour Change of Iridium(III) Bis-Terpyridine Complex Crystal Triggered by Water Sorption/Desorption

Yusuke Endo,[a] Mio Kondo,[a] Tomoe Nakamura,[a] Shingo Hattori,[a] Akiko Sekine,[b] Sosuke Kojo[b] and Kazuteru Shinozaki[a]*

[a]*Graduate School of Nanobioscience, Yokohama City University, 22-2 Seto, Kanazawa-ku, Yokohama 236-0027, Japan*
[b]*School of Science, Institute of Science Tokyo, 2-12-1 O-okayama, Meguro-ku, Tokyo 152-8551, Japan*

E-mail: shino@yokohama-cu.ac.jp

A cationic complex crystal of $[Ir(tpy)_2]Br_3 \cdot 7H_2O$ (tpy = 2,2';6',2"-terpyridine) shows a luminescence vapochromism, a reversible conversion of yellow and orange emission in response to heating/cooling. An X-ray crystallography reveals that $[Ir(tpy)_2]Br_3 \cdot 7H_2O$ is in a triclinic crystal system and constructed by Ir(III) complex layers and 2D hydrophilic sheets consisting of H_2O and Br^-. The orange emissive crystal is determined as $[Ir(tpy)_2]Br_3 \cdot 2H_2O$ in orthorhombic, where 1D hydrophilic channels consisting of H_2O and Br^- and a close approach of Br^- to Ir(III) complex are found. The yellow emission of $[Ir(tpy)_2]Br_3 \cdot 7H_2O$ is due to the dual emission from the ligand centered π-π^* state and the Br^--to-ligand charge-transfer (XLCT) state. The π-π^* emission is quenched by the switching to the XLCT emission by the close approach of Br^- to Ir(III) complex resulting from the H_2O desorption. The reversible H_2O sorption/desorption results in not only the luminescence colour change but also the drastic structural change between triclinic and orthorhombic crystal systems. The weak stimulus of H_2O sorption/desorption triggers the phase transition of Ir(III) complex crystal; $5H_2O$ squeeze into the 1D channel in $[Ir(tpy)_2]Br_3 \cdot 2H_2O$ crystal to change Ir–Br^- framework from orthorhombic to triclinic, and inversely the elimination of $5H_2O$ from the 2D hydrophilic sheet in

View Article Online
DOI: 10.1039/D6CE00194G

$[Ir(tpy)_2]Br_3 \cdot 7H_2O$ contributes to reconstruction of the hydrophilic channel along with the conversion of triclinic to orthorhombic in crystal system.

Introduction

Most crystals consisting of transition metal complexes don't lose their crystallinity and intrinsic colour even when cracked and ground into fine powders because their periodic alignments of components remain same. However, some Pt(II) complexes frequently show the loss of crystallinity resulted from amorphization upon mechanical grinding, thereby their colour and luminescence change. For example, Pt(5mdpb)Cl (5mdpbH = 1,3-di(5-methyl-2-pyridyl)benzene)[1] and Pt(5fdpb)Cl (5fdpbH = 1,3-di(5-trifluoromethyl-2-pyridyl)benzene)[2] crystals were found to show the colour change from yellow to orange associated with the switching of excited state from the π-π^* state to the MMLCT (metal metal-to-ligand charge-transfer) state of Pt-Pt dimeric form. Thereafter, the MMLCT emission of Pt(II) complex crystals based on the mechanochromism have been found.[3-11] Occasionally such a weak mechanical stimulus causes not only the dimerization of ground Pt(II) complex but also the Pt(II) complex excimer formation;[12-17] although a Pt(5mdpb)Cl (5mdpbH = 1,3-di(5-methyl-2-pyridyl)benzene) crystal[1] shows no change in the crystal structure and colour even upon mechanical grinding, it emits orange luminescence different from the original yellow before grinding. The orange luminescence is accounted for by the $(Pt\text{-}Pt)^*$ excimer formation on the surface of powdery crystals.

Another weak external-stimulus, exposure to solvent vapor, also induces colour change of Pt(II) complex crystal.[18-20] A purple crystal of Pt(Fmdpb)CN (FmdpbH = 4, 6-difuluoro-1, 3-di(5-methyl-2-pyridyl)benzene) showing no visible luminescence suddenly emits red luminescence along with red colouration upon exposure to chloroform vapor.[21] The characteristic colour change is accounted for by the emergence of visible absorption due to the MMLCT transition of a dimeric $[Pt(Fmdpb)CN]_2$ moiety resulting from the sorption of $CHCl_3$ vapor into crystal. These neutral and planar Pt(N^C^N) complex crystals exhibiting the colour change as response to mechanical grinding or exposure to $CHCl_3$ vapor are classified in "Soft Crystals",[22, 23] one of the categories of smart materials, which can easily change its structure by weak stimulus despite that its

View Article Online
DOI: 10.1039/D6CE00194G

highly ordered structure remains. So far, many materials consisting of neutral compounds including organic molecules, organometallic complexes, and transition metal complexes have been found to show the characteristics of "Soft Crystals" which is the change in morphology, colour, or luminescence as a response to weak external stimulus such as mechanical stress, exposure to vapor, or heating.[24] Recently, we presented a vapochromic behaviour of cationic complex salt $[Ir(tpy)_2]I_3 \cdot 2H_2O$ (tpy = 2,2';6',2"-terpyridine) of which colour switches between orange and red during the sorption/desorption of H_2O from/to atmosphere.[24] Reports on luminescence vapochromism of Ir(III) complex seem to be limited compared to those of Pt(II) complex.[25-31]

The strong visible colouration is due to the I^--to-tpy ligand charge-transfer (XLCT) transition of $[Ir(tpy)_2]I_3 \cdot 2H_2O$,[32] where the HOMO, a 5p orbital of I^-, is strongly influenced by the number of hydrated H_2O, resulting in the shift of the XLCT band. The X-ray crystallography of $[Ir(tpy)_2]I_3 \cdot 2H_2O$ revealed that H_2O molecules are stored in hydrophilic channels and connected with I^- by the hydrogen bonds. A Rietveld analysis of PXRD patterns for $[Ir(tpy)_2]I_3 \cdot nH_2O$ (n = 0–2) clarified that the $[Ir(tpy)_2]I_3$ moieties construct a rigid framework and remain the original packing structure during the H_2O sorption/desorption cycles.[24] Unfortunately, $[Ir(tpy)_2]I_3 \cdot nH_2O$ doesn't emit luminescence at room temperature, the vapochromic response is observed through a broad UV-vis absorption spectrum, and therefore the change in spectrum was too small to analyze the interaction of Ir(III) complex with the counter anion involved in the vapochromism. In the present work, we prepare an emissive $[Ir(tpy)_2]Br_3 \cdot 7H_2O$ to observe the luminescence vapochromic response at room temperature. The complex crystal shows a reversible luminescence colour change during the sorption/desorption of H_2O molecules along with a change in crystal structure, which is the characteristic of "Soft Crystals."

Experimental

Preparations.

$[Ir(tpy)_2]Br_3 \cdot 7H_2O$ was prepared from $[Ir(tpy)_2]I_3 \cdot 2H_2O$[24] by the ion-exchange. $[Ir(tpy)_2]I_3 \cdot 2H_2O$ (74 mg, 0.071 mmol) and AgBr (53 mg, 0.28 mmol) were dissolved in water and subsequently stirred for 1day under the dark. Removal of the white precipitate by filtration afforded a clear yellow solution. After the evaporation of solvent, the

View Article Online
DOI: 10.1039/D6CE00194G

resultant yellow solid material was washed with acetone and acetonitrile: Yield 41 mg (67%). A single crystal $[Ir(tpy)_2]Br_3 \cdot 7H_2O$ suitable for X-ray crystal structure analysis was prepared by the slow evaporation of solvent from an acetonitrile solution containing $[Ir(tpy)_2]Br_3$. Another single crystal $[Ir(tpy)_2]Br_3 \cdot 2H_2O$ suitable for X-ray crystal structure analysis was prepared by a vapor-diffusion method. To a large vial of an acetone/dimethyl sulfoxide (2:1) mixture as a poor solvent was put a small vail containing an acetonitrile solution of $[Ir(tpy)_2]Br_3$. When capped the large vial and left it to stand for 2 weeks, orange-emissive single crystals were obtained.

Measurements.

UV-vis absorption spectroscopy was conducted by using a JASCO spectrometer V-530ST. A 1 cm quartz cuvette attached with grease-less valve was used for UV-vis measurement of solid sample deposited as a thin-film on an inner wall of the cuvette. Emission spectra were measured by a JASCO FP-6500 spectrofluorometer. The samples for emission measurement were prepared in a quartz cuvette attached with a greaseless valve. Emission lifetimes were evaluated by a least squares method on a PC for time courses of luminescence recorded by a Tektronix TDS1102C digital oscilloscope after pulse excitation using a Japan Laser GL-3300 N_2 laser (337 nm). Thermogravimetry (TG) measurement was performed by using a Hitachi Hightech science STA7300. Solid sample stored in an aluminum pan was heated from 293 to 500 K at a heating rate of 5 K/min under nitrogen gas atmosphere. Differential Scanning Calorimetry (DSC) measurement was carried out in the range from room temperature to 400 K using a Hitachi Hightech science DSC 7020. A powder X-ray diffraction (PXRD) measurement was carried out by using a Bruker D8 ADVANCE equipped with a TTK450 for variable temperature measurement. PXRD patterns for $[Ir(tpy)_2]Br_3 \cdot 7H_2O$, $[Ir(tpy)_2]Br_3 \cdot 2H_2O$, $[Ir(tpy)_2]Br_3 \cdot H_2O$, and $[Ir(tpy)_2]Br_3$ were measured at 25℃, 80℃, 110℃, and 190℃, respectively. A PXRD measurement tracking the change from $[Ir(tpy)_2]Br_3 \cdot 2H_2O$ to $[Ir(tpy)_2]Br_3 \cdot 7H_2O$ was conducted at room temperature, where $[Ir(tpy)_2]Br_3 \cdot 2H_2O$ was prepared from $[Ir(tpy)_2]Br_3 \cdot 7H_2O$ by the desorption of $5H_2O$ at 80℃.

X-ray crystallography.

The X-ray diffraction data were obtained at 123 K using a Rigaku XtaLAB Synergy-DW system with MoKα radiation. Indexing, integration, scaling, and absorption correction of the diffraction data were carried out using CrysAlis^{Pro}.[33] The structure was solved by

View Article Online
DOI: 10.1039/D6CE00194G

SHELXT 2014 program[34] and refined by full-matrix least-squares techniques against F^2 (SHELXL-2019/3)[35] with the Shelxle software package.[36] All the non-hydrogen atoms were refined anisotropically. The crystal and molecular structures were drawn with the Mercury software.[37]

Results and Discussion

H_2O desorption/sorption.

A thermogravimetry (TG) measurement was conducted for a salt of $[Ir(tpy)_2]Br_3 \cdot 7H_2O$ (**M7**, tpy = 2,2':6',2"-terpyridine) prepared by an addition of acetone into an acetonitrile solution containing the Ir(III) complex. As shown in Fig. 1, the TG (black) and DTG (red) results clearly show a three-step weight loss; the peaks of DTG curve are observed at 60℃, 90℃, and 140℃. For the 1st stage, the weight change reaches -8.80% up to 65℃, which matches to the loss of $5H_2O$. Gradual decrease in weight at the beginning below 50℃ suggests that one H_2O molecule among the waters of hydration of **M7** can be easily removed from the crystal framework, which likely occurs even at room temperature. The weight changes in the 2nd and 3rd stages correspond to -1.75% and -1.76%, respectively, each of which is due to a single H_2O loss. Since there is no remarkable weight-loss in the region of 65–80℃, it is reasonably assigned that the crystal heated at 80℃ is $[Ir(tpy)_2]Br_3 \cdot 2H_2O$ (**M2**). $[Ir(tpy)_2]Br_3 \cdot H_2O$ (**M1**) and $[Ir(tpy)_2]Br_3$ (**M0**) are suggested to be obtained by the heating at 90–100℃ and 140℃, respectively. The intermediates phases of **M5**–**M3** seem not to be detected through the TG measurement. When **M0** was cooled at room temperature under humid atmosphere, the lost weight was recovered by the sorption of H_2O. Fig. S1 shows TG results for two samples experiencing the heating-cooling treatment, where the numbers of waters of hydration are determined to be 6.0 and 6.4, respectively. This result suggests that, in the H_2O sorption process from **M0** to **M7**, 6 H_2O are easily back into the crystal framework but not the last one does hardly.

View Article Online
DOI: 10.1039/D6CE00194G

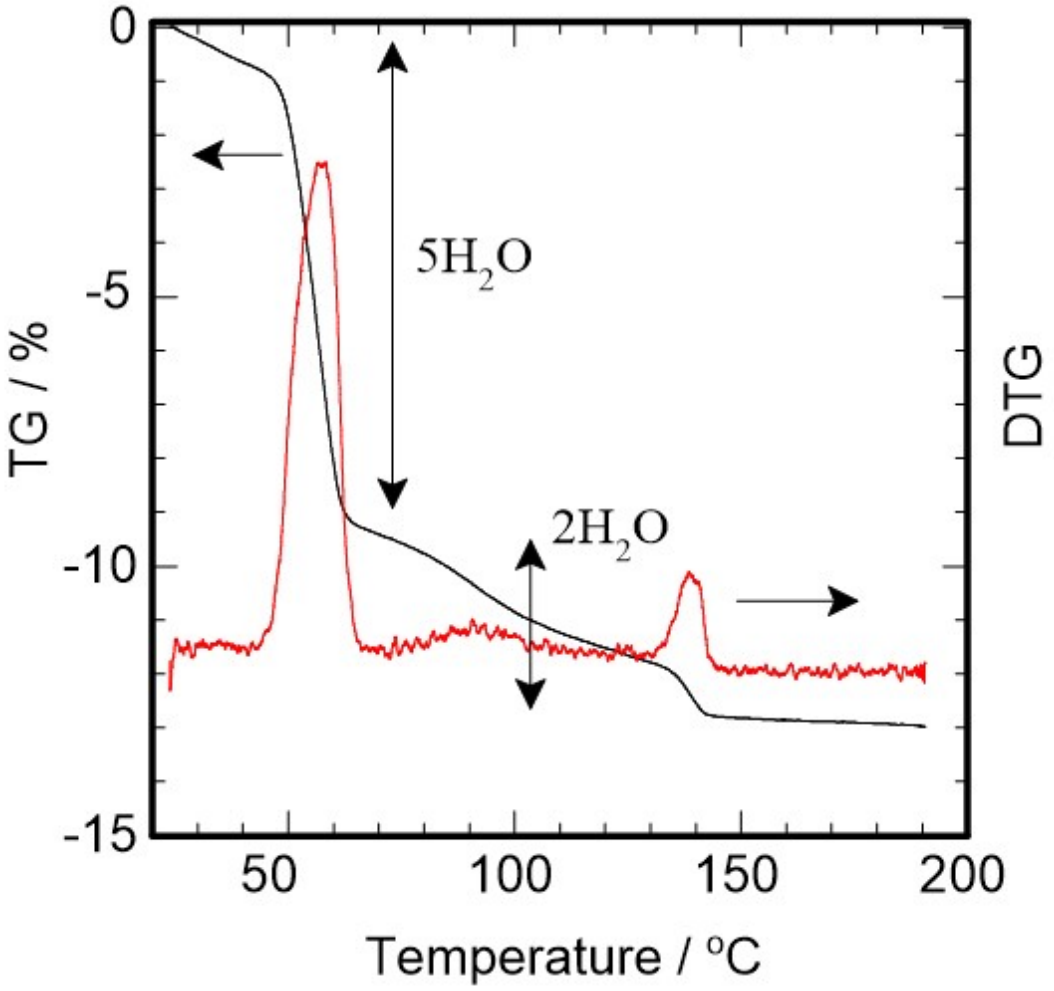

Fig. 1. TG (black) and DTG (differential TG), red for $[Ir(tpy)_2]Br_3 \cdot 7H_2O$ (**M7**). Three distinct peaks are observed at 60°C, 90°C, 140°C in the DTG curve.

Fig. S2 shows a DSC result of **M7** during heating under the N_2 atmosphere. Two distinct endothermic peaks are observed in the regions of 30–70°C and 105–125°C, which correspond to the endothermic processes for the desorption of $5H_2O$ and $2H_2O$, respectively. Since the endothermic amount at 105–125°C is +13 kJ/mol, we can estimate the endothermic amount of single H_2O desorption to be +6.5 kJ/mol. It is less than the distillation enthalpy of H_2O (ΔH = +44.016 kJ/mol at 298K),[38] suggesting that the H_2O eliminations from **M2** and **M1** easily take place. In contrast, the endothermic amount of +107 kJ/mol at 30–70°C is much larger than +32.6 kJ/mol for $5H_2O$ desorption. It is suggested that the transition from **M7** to **M2** needs a large thermal energy for the change in Ir–Br^- framework in the crystal in addition to the $5H_2O$ desorption.

View Article Online
DOI: 10.1039/D6CE00194G

Crystal structures of M7 and M2.

We determined the crystal structure of **M7** as a triclinic crystal system with *P*-1 space-group (Table S1). The X-ray diffraction study on this sample was performed at –150°C and the number of H_2O was determined to be 7 in the unit cell. When viewed from the *a*-axis of the unit cell, each Ir(III) complex aligns its principal axis of D_2 structure parallel to the *a*-axis as shown in Fig. 2. Waters of hydration are accommodated in voids between Ir(III) complexes on the *bc*-plane and make a hydrogen-bond network together with Br^-. These hydrogen-bonds are expanded along the *a*-axis to construct a 2D sheet structure. Two Br^-'s coloured with green and blue are buried in the 2D sheets, while the other (yellow) is close to Ir ($l_{Ir1–Br2}$ = 4.729 Å) and is located between two tpy ligands with a bite angle of 78.88° as to be pinched with a scissors of ligands when viewed from the (*b*–*c*)/2 axis of unit cell (Fig. S3). The Ir–Br^- pair (**A**) and its turn-over (**B**) are alternately ordered in a straight line, parallel to the hydrogen bonding networks. The distances between Br^- and O are in the range of 3.285–3.366Å and those of O–O are of 2.751–2.814 Å (Table S2). An eight-membered ring consisting of $2Br^-$ (Br1) and 6O (O4, O5, O6) is observed in the unit cell. O5 and O6 connect to O5 and O6 in the adjacent unit cells, respectively, to extend the hydrogen bonding network along the *a*-axis (Fig. S4). O1, O2, O3, and Br3 contribute to the extension of the network along the direction of (*b* – *c*)/2 axis. Br2 connects to O1 and O7 through the hydrogen bond. It is noticed that O7 makes a hydrogen bond with Br2 alone, suggesting the hydrogen bond between Br2 and O7 is weak.

View Article Online
DOI: 10.1039/D6CE00194G

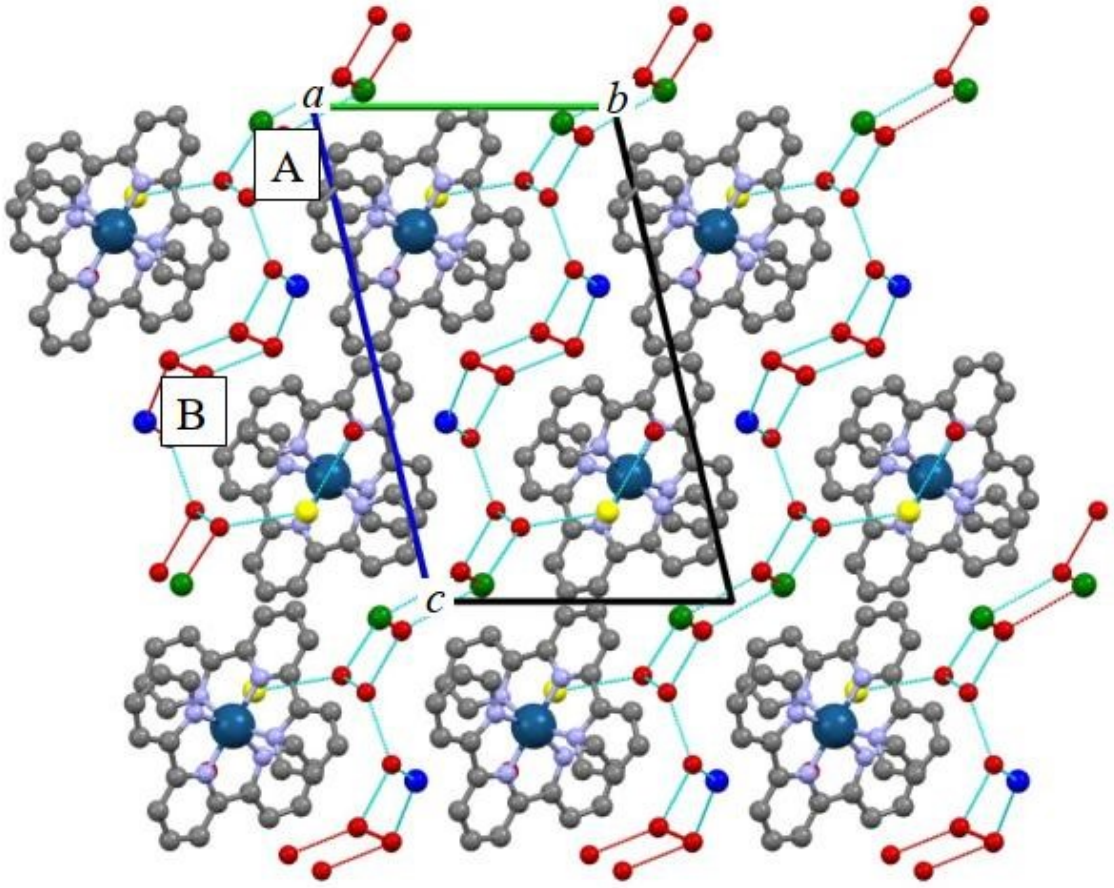

Fig. 2. Crystal structure of **M7**. **A** and **B** denote $[Ir(tpy)_2]^{3+}$-Br^- pairs. Red circles are O atoms of water of hydration. Green, yellow, and blue ones are Br^-'s. The coloured lines between O and Br show the hydrogen-bonds. Hydrogen atoms are omitted for clarity.

Another X-ray crystallography determined that the crystal system of **M2** is orthorhombic with *Pna*2_1 space-group (Table S3). As well as **M7**, two Ir–Br^- pairs (**C** and **D**) are observed in the **M2** crystal as shown in Fig. 3. Each Ir(III) complex is in almost perfect D_{2d} symmetry and aligns its principal C_2 axis parallel to the *a*-axis of the unit cell. Br^- (yellow) is located on the C_2 axis and seems not to create any hydrogen bond with H_2O. The closest distance between Br^- and Ir are determined as $l_{Ir1–Br38}$ = 4.640 Å for the Ir–Br^- pair. The pairs **C** and **D** in Fig. 3 are equivalent from each other, yet **D** is the turn-over of **C** with respect to the *bc*-plane and located with an offset of *a*/2 with respect to **C**. The other Br^-'s (green and blue) contribute to hydrogen-bonding with waters of hydration, respectively, to construct 1D channels along the *a*-axis. The distances between O and Br- are $l_{Br40\text{-}O42}$ = 3.358 Å and $l_{Br39\text{-}O41}$ = 3.355 Å, respectively (See Table S4 and Fig. S5).

View Article Online
DOI: 10.1039/D6CE00194G

The hydrogen bonds are extended along the *a*-axis of the unit cell. In addition, we found a very interesting and very rare phenomenon which is the electron deficiency around Br^- (yellow) with no hydrogen bonding (Fig. S6). Although this might be due to a partial electron transfer from Br^- to Ir(III) complex, we couldn't recognize any increase in electron density in $[Ir(tpy)_2]^{3+}$. This could be because Ir, as a heavy atom with many electrons, causes any such increase to fall within the experimental error range and thus remain undetected.

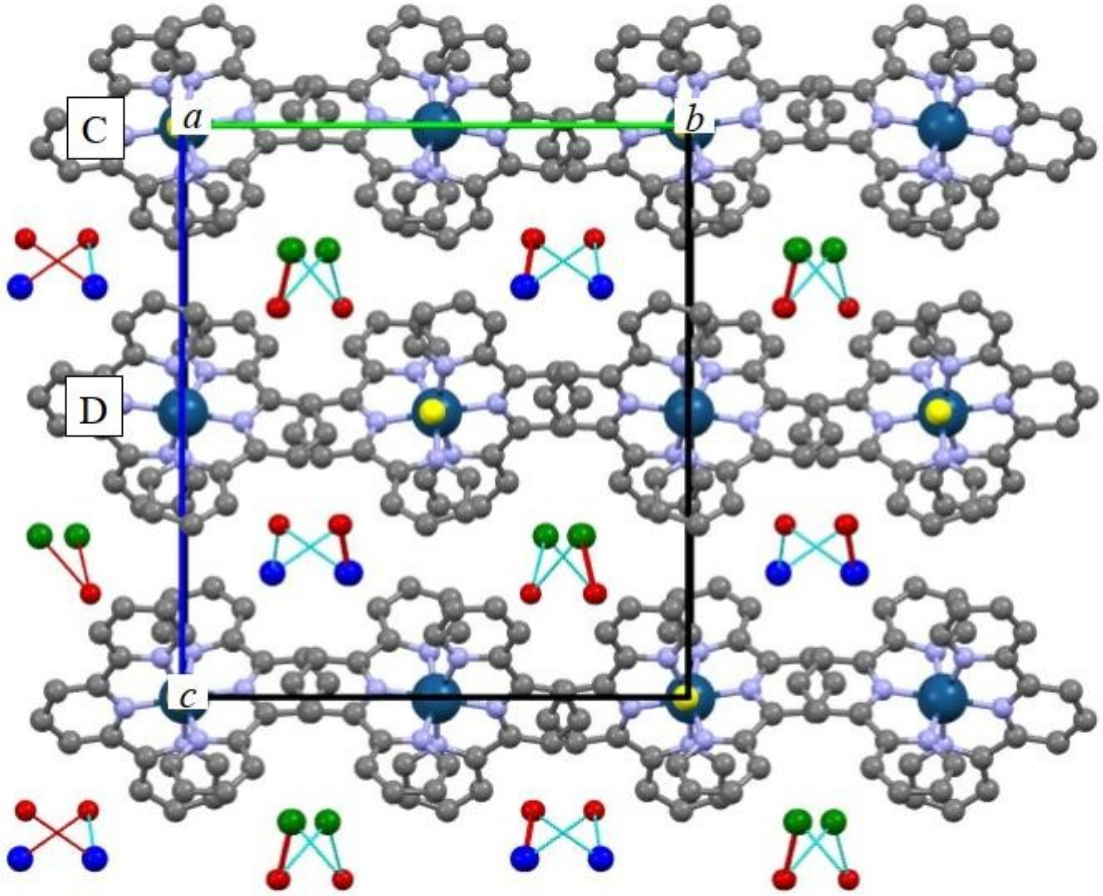

Fig. 3. Crystal structure of **M2**. **C** and **D** denote $[Ir(tpy)_2]^{3+}$–Br^- pairs. Red circles are O atoms of water of hydration. Green, yellow, and blue ones are Br's. The coloured lines between O and Br show the hydrogen-bonds. Hydrogen atoms are omitted for clarity.

The X-ray crystallography for **M7** and **M2** clarified that the difference in number of waters of hydration in crystal results in the difference in hydrogen-bond networks. H_2O can eliminate through the 2D hydrophilic sheet in the desorption process from **M7** to **M2**.

View Article Online
DOI: 10.1039/D6CE00194G

The $5H_2O$ loss results in the rearrangement of Ir–Br^- framework along with the change in hydrophilic channel from the 2D sheets to the 1D columns and with the release of $[Ir(tpy)_2]^{3+}$ from the stress due to the distorted structure. The distortion energy for the $[Ir(tpy)_2]^{3+}$ moiety was predicted through a DFT calculation[39] performed by using the CAM-B3LYP as a functional and the basis set of 6-31G* for H, C, N, O, Br, and LANL2DZ for Ir. In this calculation, the geometries for the distorted and undistorted structures were fixed to those of $[Ir(tpy)_2]^{3+}$ from the X-ray crystal structures for **M2** and **M7**, respectively, and Br^- and H_2O were omitted. The relative energy of the distorted structure in **M7** with respect to the D_{2d} structure in **M2** was predicted as +7.32 kJ/mol. Even though this exothermic energy is consumed for the conversion from **M7** to **M2**, it is too small to compensate for the endothermic energy +107 kJ/mol for the phase transition from **M7** to **M2** determined by the DSC measurement.

Rearrangement of Ir–Br^- framework.

To detect the Ir–Br^- framework change experimentally, the H_2O sorption process for **M2** was tracked through the PXRD measurement where the diffraction pattern at 2θ = 8–12° for **M2** prepared by heating at 80°C was recorded every 8 min to observe the change in peaks during the sorption of H_2O molecules by cooling. As shown in Fig. 4, three distinct peaks at 2θ = 9.4°, 10.7°, 11.5° and a small peak at 2θ = 10.4° are observed at the beginning (a, black), consistent with the powder pattern simulated from the result of the single crystal X-ray diffraction. The peaks at 9.4°, 10.4°, 11.5° gradually become small and disappear in 64 min as displayed in (b)–(j). Instead, new peaks emerge at 8.6° and 9.9° and become large by time. Eventually, three peaks at 2θ = 8.6°, 9.9°, 10.7° alone remain in the powder pattern (j). The peak shape at 10.7° seems to be not symmetric, due to the shoulder at the higher angle. These peaks are consistent with the PXRD pattern for **M7** (k). Clearly, the change in diffraction pattern corresponds to the change in Ir–Br^- framework in crystal during the H_2O sorption process from **M2** to **M7**.

Despite that this H_2O-sorption process takes around 60 min for the completion, we cannot detect any apparent peaks for **M3**–**M6**. This suggests that (1) the H_2O sorption is too rapid to detect the peaks for **M3**–**M6** by our apparatus, (2) the crystal systems of **M3**–**M6** are the same as that of **M7** or **M2**, or (3) **M3**–**M6** are not detected at all through

View Article Online
DOI: 10.1039/D6CE00194G

PXRD because of the lack of crystallinity. In the case of (1), considering that **M2** used is a powdery sample consisting of many fine crystals, the slow change in peak intensity might be due to the statistical change of **M2** content in entire fine crystals, where the rapid H_2O sorption of each fine crystal takes place. If so, any PXRD pattern should be the superposition of those of **M2** and **M7**. In the case of (2), the crystal systems of **M3**–**M6** are expected to be the same as that of **M7**. Since there is no void space in **M2** crystal to accommodate extra H_2O molecules, if H_2O molecules are forced to insert into **M2** crystal, the Ir–Br^- framework of **M2** will change to that of **M7** to accommodate extra H_2O molecules. Considering that the X-ray diffraction intensity is proportional to the number of electrons, XRD peak-intensities for **M3**–**M7** may be varied by the number of H_2O molecules even though the peaks are observed at the same angles 2θ. (Fig. S7). The observed PXRD patterns during the H_2O sorption wouldn't be reproduced from the simple superposition of those of **M2** and **M7**. Regarding the case (3), the lack of crystallinity might be provided by a variety of structural-changes in Ir–Br^- framework due to the squeezing extra H_2O molecules into **M2** crystal. In this case, the transient domains of **M3**–**M6** would contribute to the depletion of PXRD intensity.

In Fig. 4, simulations of the PXRD patterns are exhibited as coloured curves. Those of **M2** (a) and **M7** (k) were reproduced using four gauss functions and displayed as green and purple curves, respectively. For (b)–(j), the patterns simulated by the superposition of the green and purple curves are displayed as red curves, respectively, which sufficiently match to each experimental result. This concludes that the intermediate phases are not detected in the present work; that is, the H_2O sorption process along with the framework change is too rapid to detect though the PXRD measurement. Fig. S8 shows plots of composition of **M2** and **M7** in the simulation, where the change in composition is shown to be not linear nor exponential but stepwise. This result might suggest some difference in rate of framework-change depending on the inhomogeneity in crystal size of **M2**.

View Article Online
DOI: 10.1039/D6CE00194G

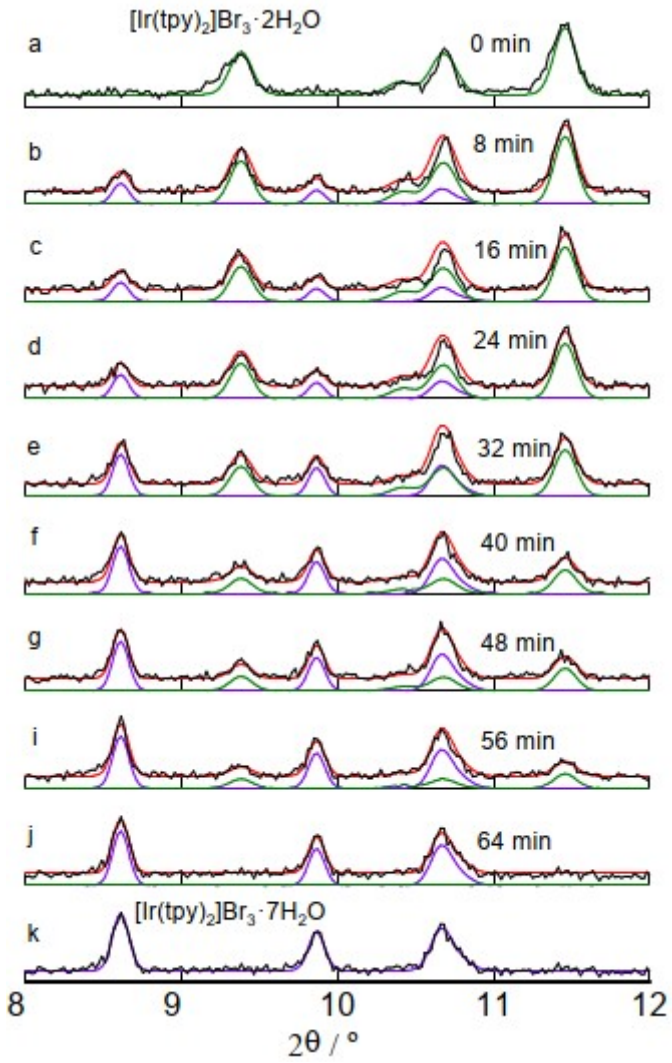

Fig. 4. A change in PXRD pattern of **M2** prepared by the heating at 80℃ upon cooling at room temperature. The diffraction patterns are observed every 8 min. For **M2** (a) and **M7** (k), each experimental PXRD pattern (black) is reproduced with four gauss functions, and the resultant simulations are displayed as green and purple, respectively. The red curves (b–i) superimposed by the simulations for **M2** (green) and **M7** (purple) are best fit to the PXRD patterns (c–k, black), respectively.

Structure of M1 and M0

A PXRD measurement carried out for $[Ir(tpy)_2]Br_3 \cdot 7H_2O$ at 190, 110, 75, 25℃, respectively. The results are exhibited as red lines in Fig. S9, where we assigned the samples at 190, 110, 75, 25℃ to **M0**, **M1**, **M2**, **M7**, respectively, according to the TG results. The blue line of **M7** is a result of simulation from the single crystal X-ray

View Article Online
DOI: 10.1039/D6CE00194G

diffraction analysis, which is in good agreement with the experimental pattern at 25℃. For **M2**, as well, the pattern observed at 75℃ is very similar to the simulation from the single crystal X-ray diffraction result, suggesting the crystal structure of Ir(III) complex prepared by heating at 75℃ from **M7** is the same as that of **M2** directly prepared by the crystallization from acetonitrile solution. This indicates that the dehydration processes from **M7** to **M2** is a single-crystal to single-crystal transition. Considering V = 1750.47 Å^3 for **M7** (Z = 2) and V = 2963.01 Å^3 for **M2** (Z = 4) from the single crystal X-ray analyses, the net difference in volume is roughly estimated as 134 Å^3 when converted into the case of Z = 1. It should be noticed that this volume difference is comparable to 150 Å^3, the sum of volumes of 5H_2O. Both the patterns of **M1** and **M0** coincide with that of **M2**, which suggests that their packing structures consisting of $[Ir(tpy)_2]^{3+}$ and $3Br^-$ are very similar to one another; that is, the crystal frameworks are robust and remain the same structure during the H_2O desorption by heating. This result suggests that the dehydration processes from **M2** to **M1** to **M0** are single-crystal to single-crystal transitions. The temperature effect on peak angles is recognized; for example, the peaks at the lowest angle are observed at 9.337° (**M2**), 9.408° (**M1**), 9.428° (**M0**). The variation of peak angles would be due to the combination of the thermal expansion of crystal lattice and the contraction resulting from the elimination of H_2O. Rietveld analyses [40] of the PXRD patterns were caried out for **M2**, **M1** and **M0**, where the geometry of It(III) complex and the space group are same as those in **M2** determined by the single crystal X-ray structural analysis. Results are in good agreement with the experimental patterns (Fig. S9). As listed in Table S5, although the lattice parameters a, b, and c decrease slightly or remain same with increasing temperature, the volumes clearly decrease. The decrease in volume from **M2** to **M0** is to be 14.8 Å^3, which is very small, considering the volume of single H_2O is 30 Å^3 and Z = 4 in the $Pna2_1$ space group. The small change in volume might guarantee the robustness of crystal framework during the sorption/desorption of H_2O.

Vapochromic behaviour.

As shown in Fig. 5, **M7** emits yellow luminescence showing vibronic structure peaking at 507, 544, 581 nm, which can be assigned to the π-π^* transition of ligand.[32] Upon heating at 80℃ for 5 min, surprisingly, the yellow luminescence changes to orange resulting in a broad spectrum centered at 623 nm. This broad emission is likely due to the Br^--to-ligand

View Article Online
DOI: 10.1039/D6CE00194G

charge-transfer (XLCT) transition of **M2**, according to the emission study on $[Ir(tpy)_2]_2X_3$ ($X^- = Cl^-, Br^-, I^-$) at 77 K.[32] The luminescence colour returns to original yellow in 40 min when the crystalline sample is cooled under ambient atmosphere. Since the luminescence change is more sensitive than the colour change, $[Ir(tpy)_2]Br_3$ crystal showing the visible luminescence vapochromism is superior to the non-emissive $[Ir(tpy)_2]I_3$ system previously reported.[32] We notice that the emission profile of **M7** looks like a superposition of the structured π-π* emission and the broad XLCT emission. This spectrum is like that of the dual emission of $[Ir(tpy)_2](PF_6)_3$ in acetonitrile,[32] where the structured and broad emission were assigned to the individual emission of $[Ir(tpy)_2]^{3+}$ and $[Ir(tpy)_3]^{3+}\cdot PF_6^-$, respectively, in the ion-association equilibrium. As well, in the present case, the broad emission component of **M7** is probably assigned to the XLCT emission of the $[Ir(tpy)_3]^{3+}\cdot Br^-$ pair, in which the Br^- bearing H_2O is located on the pseudo C_2 axis of Ir(III) complex with $l_{Ir1\text{-}Br2}$ = 4.729 Å. The broad emission of **M7** is blue shifted along with sharpening at 77K as shown in Fig. S10, which is a familiar phenomenon for CT emission of metal complexes. On the other hand, the structured π-π* emission seems to remain as a shoulder at around 500 nm even though cooling at 77 K. These results support that the emission of **M7** is assigned to the dual emission.

An emission lifetime measurement was conducted for **M7** and **M2** at room temperature. The time course of emission of **M7** monitored at 500 nm, a peak wavelength of the vibronic band of π-π* emission, consists of fast and slow decay curves (Fig. S11a); the lifetimes of the fast and slow components are estimated to be 20 ns and 300 ns, respectively, by a least square fitting using a double exponential function. When monitored at 650 nm, the peak wavelength of the broad emission, the emission lifetime was determined as τ = 540 ns, which is longer than τ = 300 ns. The longer the monitoring wavelength, the longer the emission lifetime. On the other hand, the emission lifetime of **M2** monitored at 650 nm is determined as τ = 860 ns (Fig. S11b). The H_2O desorption likely elongates the XLCT emission lifetime, probably because of the prevention from nonradiative deactivation due to the O–H vibration of H_2O. Consequently, the luminescence vapochromism of **M7** is concluded to originate from the switching the emitting state from the π-π* state to the XLCT state probably due to the close approach of Br^- to $[Ir(tpy)_2]^{3+}$.

View Article Online
DOI: 10.1039/D6CE00194G

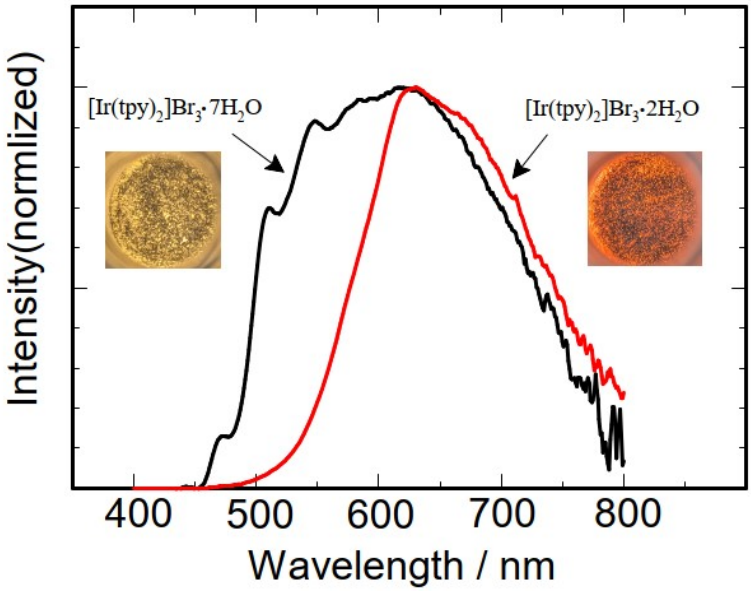

Fig. 5 Photoimages and spectra of emission from $[Ir(tpy)_2]Br_3 \cdot 7H_2O$ (**M7**) and $[Ir(tpy)_2]Br_3 \cdot 2H_2O$ (**M2**) crystals observed at room temperature.

This luminescence-colour conversion is repeatedly observed as shown in Fig. S12, plotted are the emission intensities at 540 nm of sample upon heating (red) for 10 min and cooling (black) for 20 min under humid atmosphere alternately. Although the emission intensities of heated sample are stable during the heating-cooling cycles, those after cooling seem to be varied. Fig. S13 shows a change in emission spectra of the heated sample (**M2**) observed at room temperature under humid atmosphere. The broad band at 610 nm gradually decreases in intensity along with the growth of vibronic bands in the region of 500–550 nm. The iso-emissive point observed at 570 nm at the beginning disappears eventually. By an analogy to the TG results, it is suggested that **M2** isn't converted to **M7** completely upon cooling but **M7**/**M6** mixture.

Although we cannot perceive the remarkable colour-difference in the luminescence of **M2**–**M0**, the emission measurement can detect that the emission spectrum of **M2** is slightly shifted to the longer wavelength region by removing H_2O from crystal by heating. The resultant spectra of **M1** and **M0** are like each other as shown in Fig. S14. UV absorption spectrum in the region of 250–400 nm of **M2** is also shifted to the longer wavelength region by heating to produce **M1** and **M0**. This phenomenon is very similar to that for $[Ir(tpy)_2]I_3 \cdot 2H_2O$–$[Ir(tpy)_2]I_3$ system previously found, where the reversible

View Article Online
DOI: 10.1039/D6CE00194G

colour change between yellow and orange due to the sorption/desorption of $2H_2O$ is observed.

Conclusion

We found the reversible H_2O sorption/desorption for the cationic complex crystal $[Ir(tpy)_2]Br_3 \cdot nH_2O$ (n = 7–0). The X-ray crystallography revealed the hydrophilic 2D sheets and channels in $[Ir(tpy)_2]Br_3 \cdot 7H_2O$ (triclinic) and $[Ir(tpy)_2]Br_3 \cdot 2H_2O$ (orthorhombic), respectively, both consisting of H_2O and Br^- by the hydrogen bonding. The heating of yellow $[Ir(tpy)_2]Br_3 \cdot 7H_2O$ crystal causes to remove H_2O molecules hydrated to Br^- followed by the orange colouration due to the emergence of XLCT absorption band in the visible region. This vapochromic process is accompanied by the drastic change in Ir-Br^- framework in crystal, which is a characteristic behaviour for the "Soft Crystals" and a novel phenomenon for the cationic transition metal complexes. For $[Ir(tpy)_2]Br_3 \cdot 2H_2O$, the rigidity of Ir-$Br^-$ framework makes a possible for the H_2O desorption process producing empty channels, whereas the flexibility is necessary to insert H_2O molecules into the occupied channels. It is very interesting that the weak stimulus such as an exposure to moisture causes drastic change from triclinic to orthorhombic in crystal system. Unfortunately, analysis of mechanism of the dynamic structural change from triclinic to orthorhombic was not achieved through the detection of intermediate phases for $[Ir(tpy)_2]Br_3 \cdot nH_2O$ (n = 6–3) in the present work. If it was succeeded, we would make a great contribution to the scientific understanding for "Soft Crystals," changing crystal structure upon weak external stimulus. $[Ir(tpy)_2]Br_3 \cdot 7H_2O$ was found to emit the dual emission from the π-π^* and XLCT states depending on the strength of interaction between Ir(III) complex and Br^-. The heating of $[Ir(tpy)_2]Br_3 \cdot 7H_2O$ contributes to not only the framework change but also the detachment of H_2O from hydrated Br^-. Thereby, the interaction between Ir(III) complex and Br^- is strong and stabilizes the XLCT state in energy resulting in the quenching of π-π^* emission. The switching of excited state between the π-π^* and XLCT states is one of the valuable findings in the present work.

View Article Online
DOI: 10.1039/D6CE00194G

Conflicts of interest

There are no conflicts to declare.

Data availability

The data supporting this article have been included as part of the supplementary information (SI). Supplementary information: crystallographic data, additional figures and tables. See DOI:

The crystallographic data have been deposited with the Cambridge Crystallographic Data Centre: deposition numbers CCDC 2527091 for $[Ir(tpy)_2]Br_3 \cdot 7H_2O$ and CCDC 2527097 for $[Ir(tpy)_2]Br_3 \cdot 2H_2O$. This data is provided free of charge by the Cambridge Crystallographic Data Centre.

Acknowledgements

We thank the Institute of Science Tokyo Core Facility Center for the use of the dual wavelength single crystal X-ray diffractometer (Rigaku XtaLAB Synergy-DW system). This work was supported by JSPS KAKENHI (grant numberJP21K14647).

References

1. T. Abe, T. Itakura, N. Ikeda and K. Shinozaki, Luminescence color change of a platinum(II) complex solid upon mechanical grinding, *Dalton Trans*., 2009, 711–715.
2. Y. Nishiuchi, A. Takayama, T. Suzuki and K. Shinozaki. A Polymorphic Platinum(II) Complex: Yellow, Red and Green Polymorphs and X-ray Crystallography of [Pt(fdpb)Cl] (Hfdpb = 1,3-Di(5-trifluoromethyl-2-pyridyl)benzene), *Eur. J. Inorg. Chem.*, 2011, **2011**, 1815–1823.
3. J. Ni, X. Zhang, N. Qiu, Y.-H. Wu, L.-Y. Zhang, J. Zhang, Z.-N. Chen, *Inorg. Chem.*, 2011, **50**, 9090–9096.
4. X.-P. Zhang, J.-F. Mei, J.-C. Lai, C.-H. Li, X.-Z. You, *J. Mater. Chem. C*, 2015, **3**, 2350–2357.

View Article Online
DOI: 10.1039/D6CE00194G

5. Y. Shigeta, A. Kobayashi, M. Yoshida, M. Kato, *Cryst. Growth Des.,* 2018, **18**, 3419–3427.
6. M. Martinez-Junquera, R. Lara, E. Lalinde, M. Teresa, Moreno, *J. Mater. Chem. C*, 2020, **8**, 7221–7233.
7. C.-Y. Lien, Y.-F. Hsu, Y.-H. Liu, S.-M. Peng, T. Shinmyozu and J.-S. Yang, *Inorg. Chem*. 2020, **59**, 11584–11594
8. Y. Yin, Z. Chen, R.-H. Li, C. Yuan, T.-Y. Shao, K. Wang, H. Tan and Y. Sun, *Inorg. Chem.* 2021, **60**, 9387–9393.
9. M. Martínez-Junquera, E. Lalinde and M. T. Moreno, *Inorg. Chem.* 2022, **61**, 10898–10914.
10. Y. Shigeta, T. Nomoto, M. Kato and M. Mizuno, *Inorg. Chem.* 2023, **62**, 66−74.
11. H.-H. Zhang, S.-X. Wu, Y.-Q. Wang, T.-G. Xie, S.-S. Sun, Y.-L. Liu, L.-Z. Han, X.-P. Z.-F. Shi, *Dyes and Pigments*. 2022, **197**, 109857.
12. M. Cocchi, J. Kalinowski, V. Fattori, J. A. G. Williams, L. Murphy *Appl. Phys. Lett.* **2009**, *94*, 073309.
13. S. J. Farley, D. L. Rochester, A. L. Thompson, J. A. K. Howard, J. A. G. Williams *Inorg. Chem.* **2005**, *44*, 9690–9703.
14. S. Develay, O. Blackburn, A. L. Thompson, J. A. G. Williams *Inorg. Chem.* **2008**, *47*, 11129–11142.
15. M. Cocchi, D. Virgili, V. Fattori, D. L. Rochester and J. A. G. Williams *Adv. Funct. Mater.* **2007**, *17*, 285–289.
16. W. Mróz, C. Botta, U. Giovanella, E. Rossi, A. Colombo, C. Dragonetti, D. Roberto, R. Ugo, A. Valore and J. A. G. Williams *J. Mater. Chem.*, **2011**, *21*, 8653–8661
17. M. Cocchi, J. Kalinowski, V. Fattori, J. A. G. Williams and L. Murphy *Appl. Phys. Lett.* **2009**, *94*, 073309.
18. N. M. Barker, S. D. Taylor, E. Ferguson, J. A. Krause, A. G. Oliver, W. B. Connick and P. Zhang, *Inorg. Chem.* 2021, **60**, 14731–14743.

View Article Online
DOI: 10.1039/D6CE00194G

19. C. L. Stubbs, M. J. Bryant, L. E. Hatcher and P. R. Raithby, *CrystEngComm*, 2025, **27**, 7498–7513.
20. Y. Li, L. Chen, Y. Ai, E. Y.-H. Hong, A. K.-W. Chan and V. W.-W. Yam, *J. Am. Chem. Soc*. 2017, **139**, 13858–13866.
21. S. Hattori, T. Nakano, N. Kobayashi, Y. Konno, E. Nishibori, T. Galica and K. Shinozaki, *Dalton Trans.*, 2022, **51**, 15830–15841.
22. M. Kato and K. Ishii, Soft Crystals: Flexible Response Systems with High Structural Order (The Materials Research Society Series), Springer, 2023.
23. M. Kato, H. Ito, M. Hasegawa and K. Ishii, *Chem. Eur. J.*, 2019, **25**, 5105–5112.
24. S. Hattori, M. Kondo, A. Sekine and K. Shinozaki, Vapochromism of an iridium(III) bis-terpyridine complex based on the modulation of halide-to-ligand charge transfer transition, *Dalton Trans.*, 2022, **51**, 7068–7075.
25. P. Alam, M. Karanam, D. Bandyopadhyay, A. R. Choudhury and I. R. Laskar, *Eur. J. Inorg. Chem.* 2014, 3710–3719.
26. P. Alam, M. Karanam, D. Bandyopadhyay, A. R. Choudhury and I. R. Laskar, *Eur. J. Inorg. Chem.* 2014, 3710–3719.
27. E. V. Nykhrikova, M. A. Kiseleva, P. Kalle, S. S. Mariasina, S. A. Kozyukhin, S. V. Tatarin and S. I. Bezzubov, *Inorg. Chem*. 2025, **64**, 5210–5220.
28. X. Zhu, P. Cui, S. Kilina and W. Sun, *Inorg. Chem*. 2017, **56**, 13715–13731.
29. P. Bolle, H. Serier-Brault, R. Génois, E. Faulques, A. Boulmier, O. Oms, M. Lepeltier, J. Marrot, A. Dolbecq, P. Mialane and R. Dessapt, *J. Mater. Chem. C*, 2016, **4**, 11392–11395.
30 Y. Jiang, G. Li, D. Zhu, Z. Su and M. R. Bryce, *J. Mater. Chem. C*, 2017, **5**, 12189–12193.
31. Y. Wang, T. Yang, X. Liu, G. Li, W. Che, D. Zhu and Z. Su, *J. Mater. Chem.* C, 2018, **6**, 12217–12223.
32. W. Ito, S. Hattori, M. Kondo, H. Sakagami, O. Kobayashi, T. Ishimoto and K. Shinozaki, Dual Emission from an Iridium(III) Complex/Counter Anion Ion Pair, *Dalton Trans.*, 2021, **50**, 1887–1894.
33. CrysAlisPro : Agilent Technologies Ltd, Yarnton, Oxfordshire, England, 2014.

View Article Online
DOI: 10.1039/D6CE00194G

34. G. M. Sheldrick, SHELXT – Integrated space-group and crystal-structure determination, *Acta Cryst*., 2015, **A71**, 3–8.

35. G. M. Sheldrick, Crystal structure refinement with SHELXL, *Acta Cryst.*, 2015, **C71**, 3–8.

36. C. B. Hübschle, G. M. Sheldrick and B. Dittrich, ShelXle: a Qt graphical user interface for SHELXL, *J. Appl. Crystallogr*., 2011, **44**, 1281–1284.

37. C. F. Macrae, P. R. Edgington, P. McCabe, E. Pidcock, G. P. Shields, R. Taylor, M. Towler and J. van de Streek, Mercury: visualization and analysis of crystal structures, *J. Appl. Crystallogr.*, 2006, **39**, 453–457.

38. P. Atkins and J. de Paula, Atkins' Physical Chemistry 9th Ed., Oxford New York, 2010.

39. Gaussian 16, Revision C.01, M. J. Frisch, G. W. Trucks, H. B. Schlegel, G. E. Scuseria, M. A. Robb, J. R. Cheeseman, G. Scalmani, V. Barone, G. A. Petersson, H. Nakatsuji, X. Li, M. Caricato, A. V. Marenich, J. Bloino, B. G. Janesko, R. Gomperts, B. Mennucci, H. P. Hratchian, J. V. Ortiz, A. F. Izmaylov, J. L. Sonnenberg, D. Williams-Young, F. Ding, F. Lipparini, F. Egidi, J. Goings, B. Peng, A. Petrone, T. Henderson, D. Ranasinghe, V. G. Zakrzewski, J. Gao, N. Rega, G. Zheng, W. Liang, M. Hada, M. Ehara, K. Toyota, R. Fukuda, J. Hasegawa, M. Ishida, T. Nakajima, Y. Honda, O. Kitao, H. Nakai, T. Vreven, K. Throssell, J. A. Montgomery, Jr., J. E. Peralta, F. Ogliaro, M. J. Bearpark, J. J. Heyd, E. N. Brothers, K. N. Kudin, V. N. Staroverov, T. A. Keith, R. Kobayashi, J. Normand, K. Raghavachari, A. P. Rendell, J. C. Burant, S. S. Iyengar, J. Tomasi, M. Cossi, J. M. Millam, M. Klene, C. Adamo, R. Cammi, J. W. Ochterski, R. L. Martin, K. Morokuma, O. Farkas, J. B. Foresman, and D. J. Fox, Gaussian, Inc., Wallingford CT, 2016.

40. F. Izumi and K. Momma, *Solid State Phenom.*, 2007, **130**, 15–-20.

View Article Online
DOI: 10.1039/D6CE00194G

Data availability

The data supporting this article have been included as part of the supplementary information (SI). Supplementary information: crystallographic data, additional figures and tables. See DOI:

The crystallographic data have been deposited with the Cambridge Crystallographic Data Centre: deposition numbers CCDC 2527091 for $[Ir(tpy)_2]Br_3 \cdot 7H_2O$ and CCDC 2527097 for $[Ir(tpy)_2]Br_3 \cdot 2H_2O$. This data is provided free of charge by the Cambridge Crystallographic Data Centre.